Semiannual and solar activity variations of daytime plasma observed by DEMETER in the ionosphere-plasmasphere transition region

Liuyuan Li, Jinbin Cao, Junying Yang, Jean-Jacques Berthelier, Jean-Pierre Lebreton

AGU PUBLICATIONS

JGR

Journal of Geophysical Research: Space Physics

RESEARCH ARTICLE
10.1002/2015JA021102

Key Points:
- Semiannual variation of the daytime heavy oxygen ions is mainly controlled by neutral atomic oxygen
- Semiannual variations of light ions (He^+ and H^+) depend on their neutral sources and external forces
- Neutral composition densities also affect their ion concentrations during different solar activities

Correspondence to:
L. Y. Li,
lyli_ssri@buaa.edu.cn

Citation:
Li, L. Y., J. B. Cao, J. Y. Yang, J. J. Berthelier, and J.-P. Lebreton (2015), Semiannual and solar activity variations of daytime plasma observed by DEMETER in the ionosphere-plasmasphere transition region, *J. Geophys. Res. Space Physics*, *120*, doi:10.1002/2015JA021102.

Received 8 FEB 2015
Accepted 9 NOV 2015
Accepted article online 11 NOV 2015

Semiannual and solar activity variations of daytime plasma observed by DEMETER in the ionosphere-plasmasphere transition region

L. Y. Li[1], J. B. Cao[1], J. Y. Yang[1], J. J. Berthelier[2], and J.-P. Lebreton[3]

[1]School of Astronautics, Beihang University, Beijing, China, [2]LATMOS/IPSL, UPMC, Paris, France, [3]LPC2E/CNRS/Universite d'Orleans, Orleans, France

Abstract Using the plasma data of Detection of Electro-Magnetic Emissions Transmitted from Earthquake Regions (DEMETER) satellite and the NRLMSISE-00 atmospheric model, we examined the semiannual and solar activity variations of the daytime plasma and neutral composition densities in the ionosphere-plasmasphere transition region (~670–710 km). The results demonstrate that the semiannually latitudinal variation of the daytime oxygen ions (O^+) is basically controlled by that of neutral atomic oxygen (O), whereas the latitude distributions of the helium and hydrogen ions (He^+ and H^+) do not fully depend on the neutral atomic helium (He) and hydrogen (H). The summer enhancement of the heavy oxygen ions is consistent with the neutral O enhancement in the summer hemisphere, and the oxygen ion density has significantly the summer-dense and winter-tenuous hemispheric asymmetry with respect to the dip equator. Although the winter enhancements of the lighter He^+ and H^+ ions are also associated with the neutral He and H enhancements in the winter hemisphere, the high-density light ions (He^+ and H^+) and electrons (e^-) mainly appear at the low and middle magnetic latitudes ($|\lambda| < 50°$). The equatorial accumulations of the light plasma species indicate that the light charged particles (He^+, H^+, and e^-) are easily transported by some equatorward forces (e.g., the magnetic mirror force and centrifugal force). The frequent Coulomb collisions between the charged particles probably lead to the particle trappings at different latitudes. Moreover, the neutral composition densities also influence their ion concentrations during different solar activities. From the low-$F_{10.7}$ year (2007–2008) to the high-$F_{10.7}$ year (2004–2005), the daytime oxygen ions and electrons increase with the increasing neutral atomic oxygen, whereas the daytime hydrogen ions tend to decrease with the decreasing neutral atomic hydrogen. The helium ion density has no obvious solar activity variation, suggesting that the generation (via the neutral He photoionization) and loss (via the charge exchange with neutral nitrogen N_2 and/or the recombination with electrons) of the daytime He^+ ions are comparable during different solar activities.

1. Introduction

The Earth's topside ionosphere (~600–1100 km) is a transition region between ionosphere (where O^+ is the dominant ion) and plasmasphere (where H^+ become dominant) [*MacPherson et al.*, 1998; *Heelis et al.*, 2009; *Yue et al.*, 2010; *Nanan et al.*, 2012; *Aponte et al.*, 2013]. In this transition region, different ions (O^+, He^+, and H^+) and electrons (e^-) mainly come from the ionization of neutral atmospheric compositions through absorption of solar extreme ultraviolet (EUV) radiation, and some plasma species are also lost through the charge exchange or recombination reactions [*Weiss*, 1953; *Schunk and Nagy*, 2009]. Besides the photochemical reactions, the plasma spatial distributions are changed by neutral wind drag and/or electromagnetic forces [*Anderson*, 1973; *Murphy et al.*, 1984; *Balan et al.*, 2013; *Denton et al.*, 2002; *Luan and Solomon*, 2008; *Wang et al.*, 2015]. Meanwhile, the plasma motions are also influenced by magnetosphere-ionosphere coupling processes [*Song et al.*, 2001, 2009; *Song and Vasyliūnas*, 2013; *Tu et al.*, 2014]. The ionospheric ions may outflow into the magnetosphere [*Yu and Ridley*, 2013a] and therefore influence some dynamic processes in the magnetosphere [*Li et al.*, 2011a; *Yu and Ridley*, 2013b].

Previous observations at different altitudes indicate that the ionospheric plasma has diurnal variation, 27 day variation, and seasonal variation [*Taylor et al.*, 1970; *Rich et al.*, 2003; *Su et al.*, 2005; *Horvath and Lovell*, 2009a, 2009b; *Liu et al.*, 2009]. However, the semiannually changed spatial morphologies of different plasma species and the relevant chemical and dynamical processes are not yet fully understood,

owing to the lack of detailed comparisons between the semiannually changed plasma species and its neutral source in the same region. Moreover, the cause of the solar activity variation of the ionospheric plasma is also unclear, although the $F_{10.7}$-dependent variations of some plasma species have been observed by radars or satellites [*Liu et al*., 2006, 2007a, 2007b; *Chen et al*., 2009; *Borgohain and Bhuyan*, 2010; *Gladyshev et al*., 2012].

In this study, we examined the semiannual and solar activity variations of the daytime plasma and neutral composition densities at ~670–710 km during different phases of solar activity (2004–2005 and 2007–2008). The results demonstrate that the semiannually latitudinal variation of the daytime oxygen ions (O^+) is basically controlled by that of neutral atomic oxygen (O), whereas the latitude distributions of the helium and hydrogen ions (He^+ and H^+) do not fully depend on the neutral atomic helium (He) and hydrogen (H). Moreover, we also found that the neutral atmospheric composition densities also influence their ion concentrations during different solar activities ($F_{10.7}$).

2. Data Source

In this paper, the plasma density and temperature are measured by the Detection of Electro-Magnetic Emissions Transmitted from Earthquake Regions (DEMETER) satellite at ~670–710 km during the declining phase of solar activity (17 November 2004 to 21 March 2005) and solar minimum (21 March 2007 to 21 March 2008). The DEMETER satellite was launched into a Sun-synchronous circular orbit on 29 June 2004. Its initial orbit altitude was ~710 km before December 2005 and thereafter declined to ~670 km. The equatorial crossing local times (LT) of DEMETER are 10:30 A.M. and 22:30 P.M.

The thermal plasma analyzer (Instrument d'Analyse du Plasma (IAP)) on board DEMETER can measure the density and temperature (~10^2 to 5×10^3 K) of the ions O^+, H^+, and He^+ [*Berthelier et al*., 2006], and the absolute accuracy of the measured ion density is better than 15% [*Wang et al*., 2010]. Moreover, the Langmuir probe experiment (Instrument Sonde de Langmuir (ISL)) on board DEMETER can measure the electron density ($[e^-]$) and temperature (~10^2 to 6×10^3 K) [*Lebreton et al*., 2006], and the absolute error on the measured electron density is about 20% to 25% [*Wang et al*., 2010]. Although the errors can influence the measured values of plasma densities, their influences are negligible for the relative variations of the semiannually or annually averaged plasma densities in our study.

Based on the criterion of charge neutrality ($[e^-]=[O^+]+[H^+]+[He^+]$), we selected the dayside plasma data measured under quiet geomagnetic conditions (geomagnetic indices $Kp\le3$, $Dst\ge-30$ nT, and $AE\le200$ nT) and calculated their semiannual and annual means in longitude-latitude grids ($4°\times2°$). The referenced geomagnetic indices (*Kp*, *Dst*, and *AE*) and the daily 10.7 cm solar radio flux ($F_{10.7}$) come from the OMNI database in the Coordinated Data Analysis Web. The number density and temperature of the neutral atmospheric compositions are obtained from the NRLMSISE-00 atmospheric model [*Picone et al*., 2002]. The annual and semiannual variations of thermospheric density in the NRLMSISE-00 model have been found to agree fairly well with the CHAMP and Gravity Recovery and Climate Experiment observations at 400 km [*Lei et al*., 2012].

3. Comparative Analysis

3.1. Semiannual Variations of the Daytime Plasma and Neutral Compositions

Semiannual means of the daytime plasma densities in longitude-latitude grids ($4°\times2°$) can reflect their semiannual variations from northern summer (21 March to 23 September) to southern summer (23 September to 21 March). Figure 1 shows the semiannual variations of the daytime (~ 10:30 LT) plasma densities observed by DEMETER at ~670 km during solar minimum (21 March 2007 to 21 March 2008). The average of $F_{10.7}$ is about 72×10^{-22} W m^{-2} Hz^{-1} in the solar minimum. The DEMETER data effectively covered the magnetic latitudes (λ) inside the plasmapause (λ_{PP}). The plasmapause latitude (λ_{PP}) is obtained from an empirical plasmapause model [*Moldwin et al*., 2002]. The dip equator (λ_{dip}) corresponds to the magnetic latitude where the magnetic inclination $I\sim0$ in the International Geomagnetic Reference Field (IGRF) magnetic field model. For most magnetic longitudes (φ), the dip equator is the same as the magnetic equator ($\lambda\sim0°$), namely, $\lambda_{dip}\sim0°$. However, the dip equator has a large northward deviation ($\lambda_{dip}\sim15°$) in the South Atlantic Magnetic Anomaly (SAMA) region ($-70°\le\lambda\le-10°$ and $0°\le\varphi\le120°$).

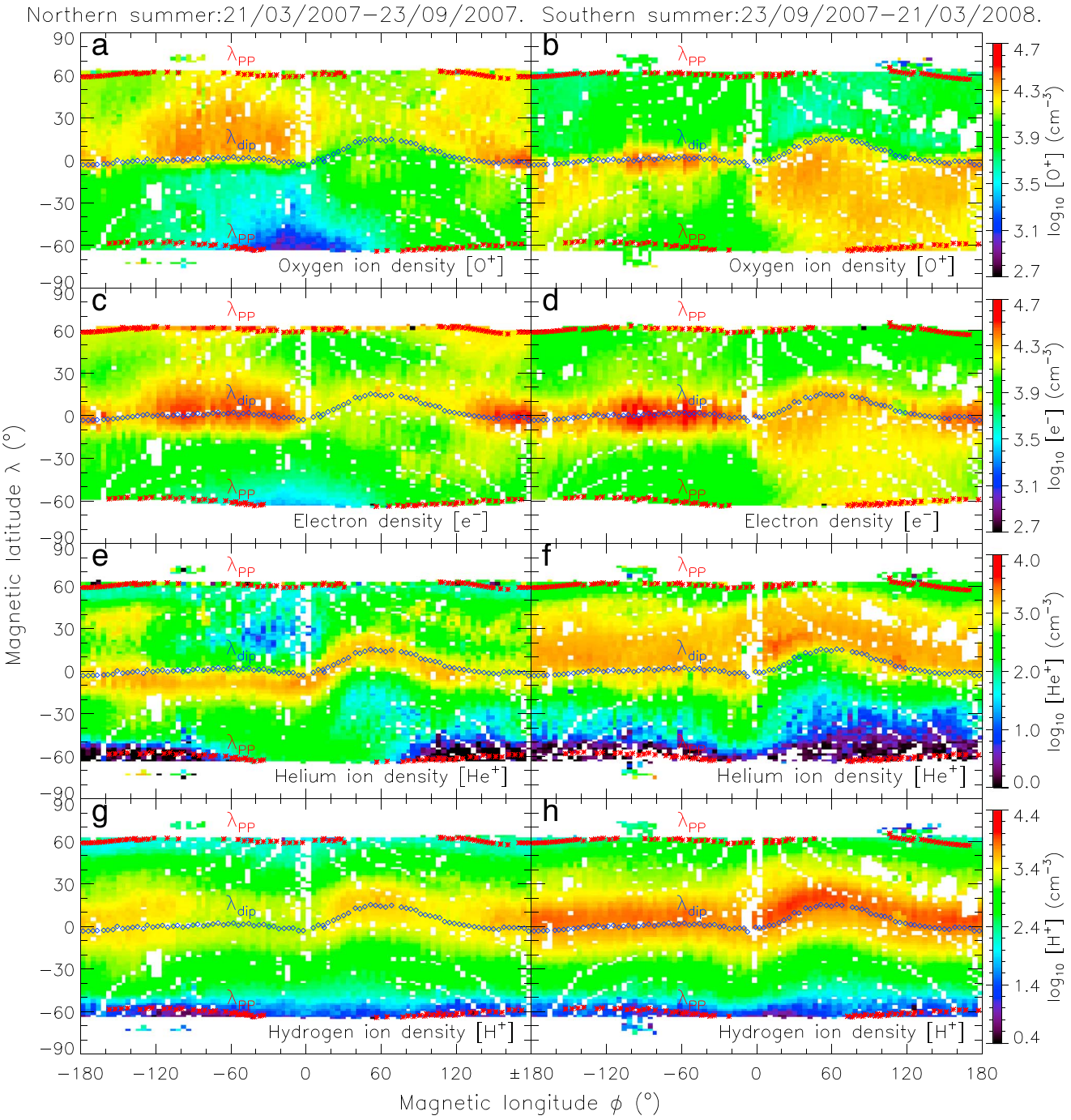

Figure 1. Semiannual variations of daytime (~10:30 LT) plasma densities observed by DEMETER at ~670 km during solar minimum (21 March 2007 to 21 March 2008). λ_{dip} (blue diamond) is the dip equator where the magnetic declination $I \sim 0$, and it is obtained from the IGRF magnetic field model. λ_{PP} (red asterisk) is the plasmapause location from an empirical model [*Moldwin et al.*, 2002].

Interestingly, the spatial distributions of all plasma species are mainly controlled by the dip equator (λ_{dip}) rather than the magnetic equator ($\lambda \sim 0°$). From the northern summer (Figures 1a, 1c, 1e, and 1g) to the southern summer (Figures 1b, 1d, 1f, and 1h), the daytime oxygen ions always increase (density $[O^+] \geq 10^{4.2}\,cm^{-3}$) on the summerside of the dip equator (indicated by Figures 1a and 1b), and their latitude distribution has significantly the summer-dense and winter-tenuous hemispheric asymmetry with respect to the dip equator, except for the low density (i.e., the small $[O^+]$) in the Weddell Sea Anomaly (WSA) region ($-70° \leq \lambda \leq -20°$ and $-120° \leq \varphi \leq 0°$)

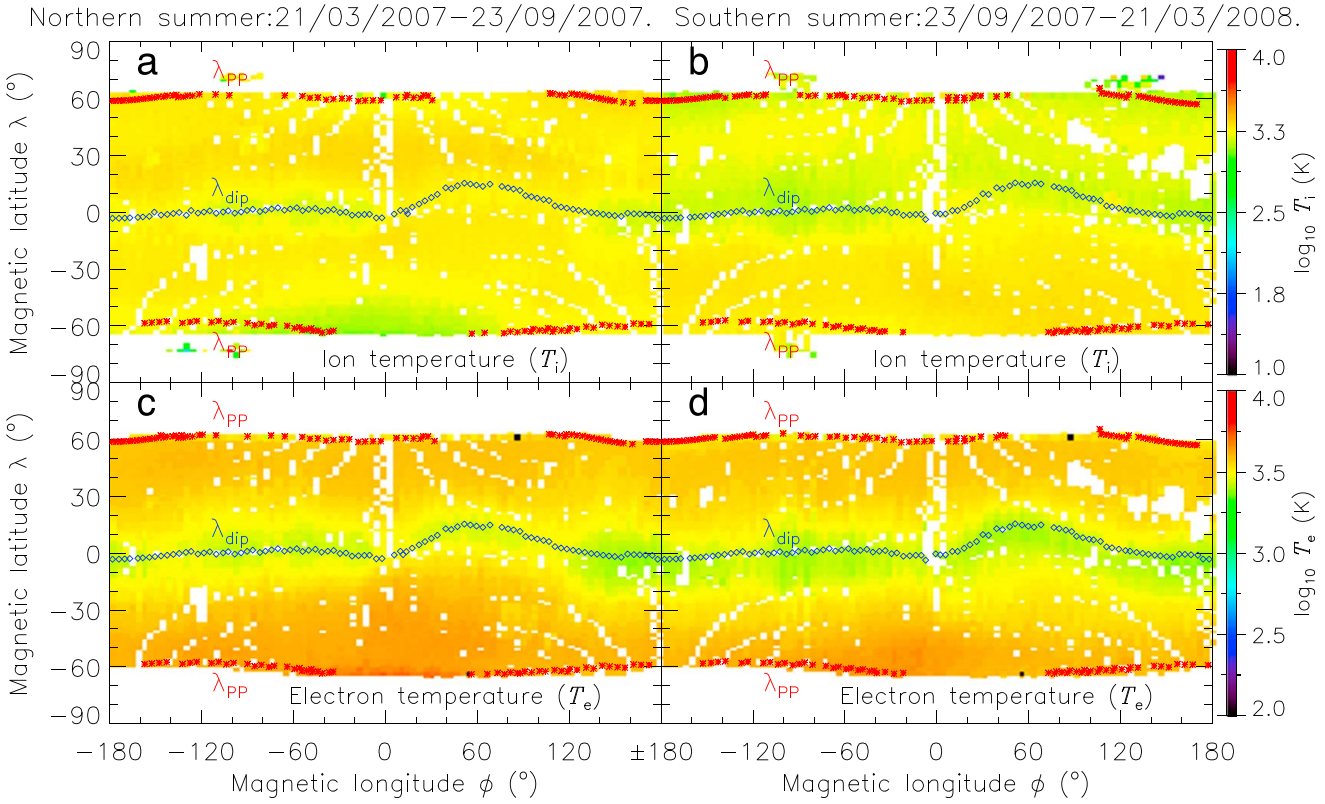

Figure 2. Daytime (~10:30 LT) plasma temperatures observed by DEMETER at ~670 km during the northern and southern summers.

[*Li et al.*, 2011b]. Although the electron number density [e^-] also tends to increase in the summer hemisphere, the highest electron density ([e^-] ~ $10^{4.6}$ cm^{-3}) appears around the dip equator (indicated by Figures 1c and 1d).

Unlike the semiannual variation of the heavy oxygen ions, the daytime helium ions (He^+) with a lighter mass often increase ([He^+] ≥ 10^3 cm^{-3}) at the low and middle magnetic latitudes ($|\lambda| < 50°$) on the winterside of the dip equator, and the helium ion density ([He^+]) has the winter-dense and summer-tenuous hemispheric asymmetry with respect to the dip equator. However, the daytime hydrogen ions (H^+) with the lightest mass can accumulate at low latitudes ($|\lambda| < 30°$) in both hemispheres and therefore maintain a maximum density ([H^+] ≥ $10^{3.4}$cm^{-3}) around the dip equator. The multiple-species plasma measurements by DEMETER demonstrate that the dayside latitude distributions of different mass plasma species can display different semiannual variations at the transition altitude of ~670 km.

In contrast to the semiannually latitudinal variation of plasma density, the latitude distribution of plasma temperature is relatively stable at ~670 km. Figure 2 displays the ion and electron temperatures (T_i and T_e) during the northern and southern summers. The ion and electron temperatures are higher at middle-to-high latitudes than the dip equator region. Comparing Figure 1 with Figure 2, we found that the ion temperature has little influence on their densities. This is consistent with the small change in simulated ion flux for various temperatures above 500 K [*Chao and Su*, 2000]. However, the electron density is inversely proportional to its temperature measured by the ISL [*Lebreton et al.*, 2006]. The maximum electron density around the dip equator is similar to the ROCSAT-1 observations at 600 km [*Chen et al.*, 2009].

Since the ionospheric plasma is produced or lost mainly through the neutral gas photoionization or charge exchange reaction [*Torr and Torr*, 1978; *Denton et al.*, 2002; *Schunk and Nagy*, 2009], we investigated the semiannual variation of neutral composition density along the dayside DEMETER path. Figure 3 shows the temperature and density of neutral atmospheric compositions at ~670 km on the dayside (~10:30 LT) during the solar minimum (21 March 2007 to 21 March 2008). The neutral temperature and density are averaged in all longitudes. The neutral composition temperature (T_n) always increases in the summer hemisphere

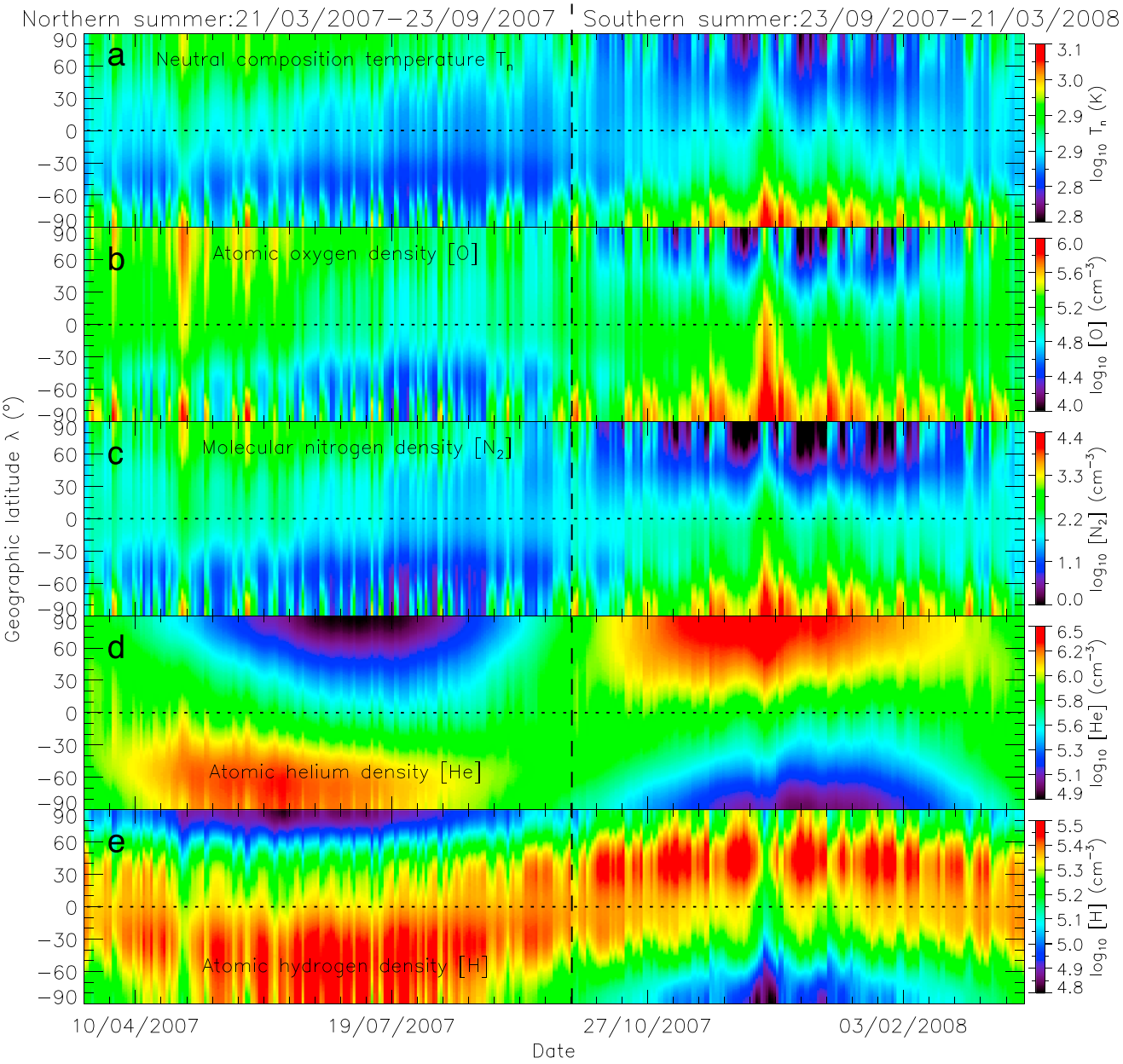

Figure 3. Semiannual variations of the (a) temperature and (b–e) density of neutral atmospheric compositions at ~670 km on the dayside (~10:30 LT) during solar minimum. The neutral temperature and densities are obtained from the NRLMSISE-00 atmospheric model [*Picone et al.*, 2002], and they are averaged in all longitudes.

(Figure 3a), and the highest neutral temperature is in the polar region (>60°). The summer increase of the neutral composition temperature is consistent with the direct sunlight and polar day in the summer hemisphere. Owing to the summer thermal expansion of the low-altitude dense atmosphere, the neutral atomic oxygen (density [O]) and molecular nitrogen ([N_2]) increase in the high-temperature summer hemisphere (corresponding to a raise in the scale height of neutral compositions, $H_n = \frac{2kT_n}{m_n g}$, where k is Boltzmann's constant, m_n is the neutral composition mass, and g is the gravitational acceleration). On the contrary, the neutral atomic helium (He) and hydrogen (H) with lighter masses often increase in the winter hemisphere (Figures 3d and 3e). The winter helium bulge has been observed by the Atmosphere Explorer D satellite, and the winter enhancements of the light neutral H and He are due to the cross-equator winds blowing from the summer hemisphere to the winter hemisphere [*Mauersberger et al.*, 1976]. However, the heavy neutral O and N_2 are not easily

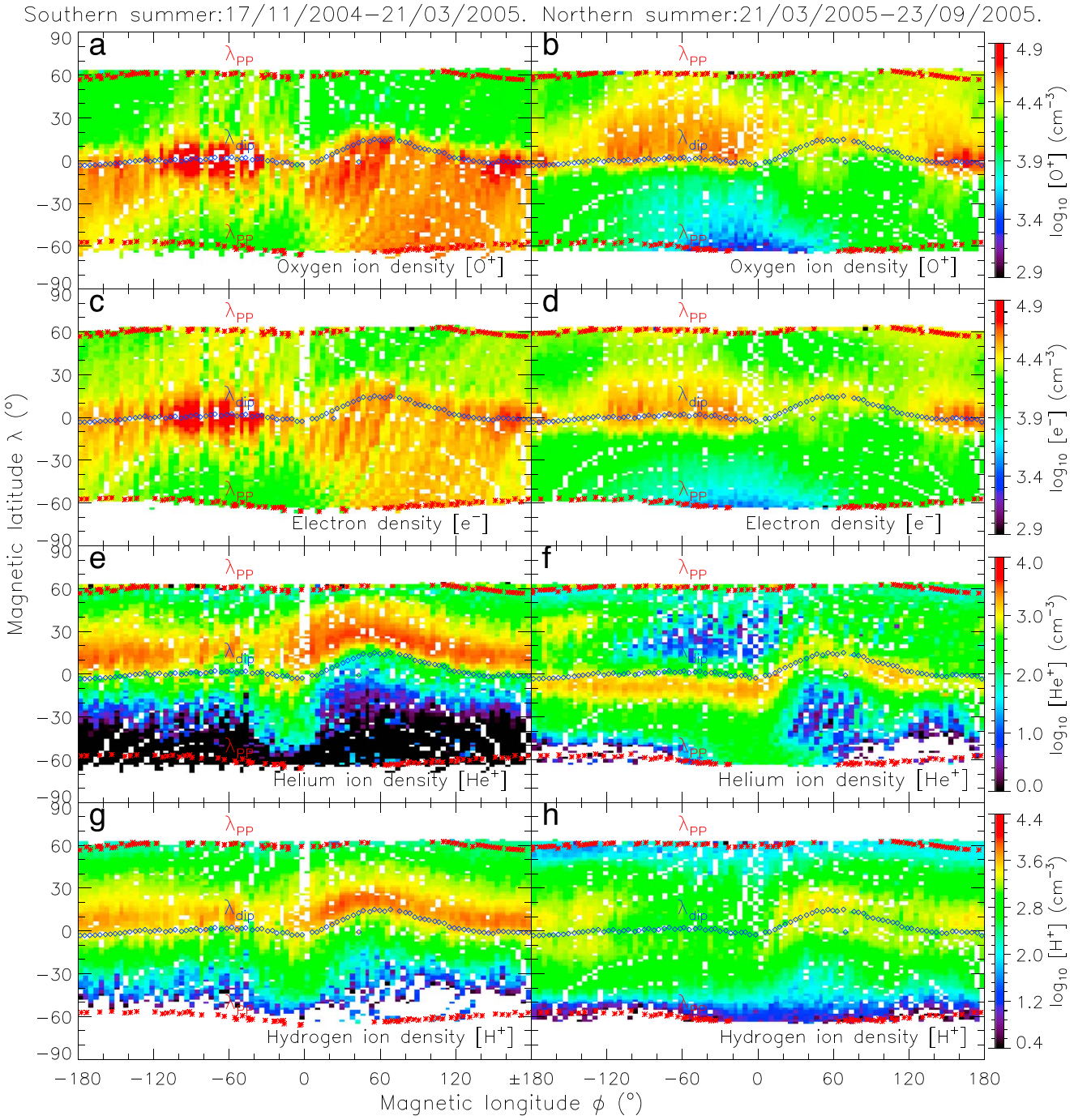

Figure 4. Semiannual variations of daytime (~10:30 LT) plasma densities observed by DEMETER at ~710 km during declining phase of solar activity (17 November 2004 to 23 September 2005).

moved under the same neutral wind drag ($F_n = m_n a_n$. The larger the neutral mass (m_n) is, the smaller the acceleration (a_n) is).

The semiannual enhancement of the neutral O density (Figure 3b) in the summer hemisphere is consistent with that of the daytime O^+ density (Figures 1a and 1b), indicating that the photoionization of the summer-increasing neutral atomic oxygen ($O + h\upsilon \rightarrow O^+ + e^-$) is mainly responsible for the oxygen ion enhancements on the summerside. Although the winter-increasing neutral helium (He) or hydrogen (H) can also produce more He^+ and H^+ ions in the winter hemisphere through the photoionization ($He + h\upsilon \rightarrow He^+ + e^-$) and charge

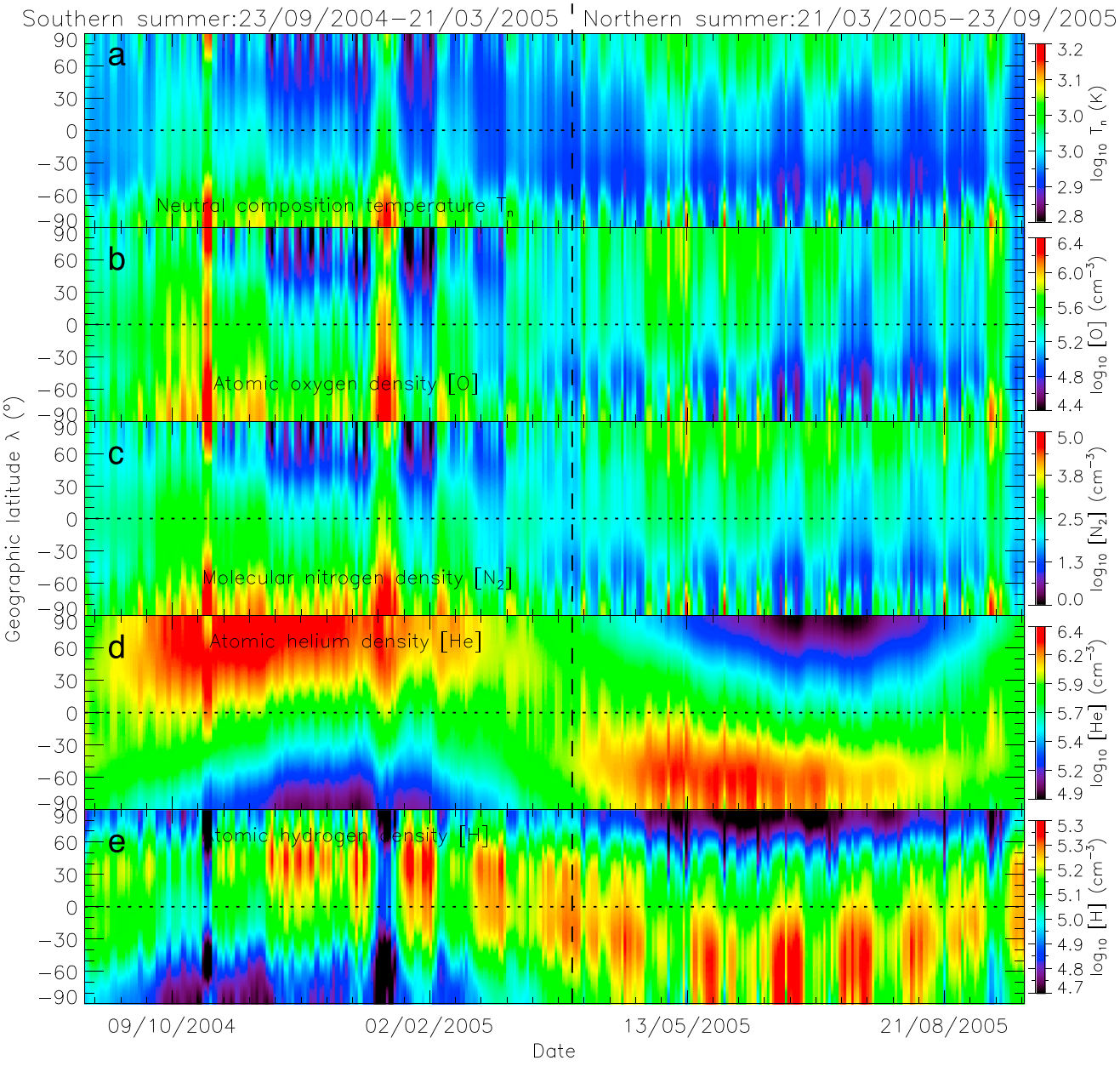

Figure 5. Semiannual variations of the (a) temperature and (b–e) density of neutral atmospheric compositions at ~ 710 km on the dayside (~10:30 LT) during declining phase of solar activity.

exchange reaction ($H + O^+ \leftrightarrow H^+ + O$), the latitude distributions of the high-density He^+ and H^+ ions are not fully determined by the high-density neutral He and H in the transition region. Therefore, only photochemical reactions cannot fully explain the spatial distributions of the light plasma species ([e^-], [H^+], and [He^+]). The equatorial maximum densities of the light plasma species are probably due to other dynamic processes (discussed in section 4).

The different plasma species have also different semiannual variations during the declining phase of solar activity. Figures 4 and 5 show the semiannual variations of the daytime (~10:30 LT) plasma and neutral densities at ~ 710 km during the interval from 17 November 2004 to 23 September 2005 (the averaged $F_{10.7}$ is about 97×10^{-22} W m^{-2} Hz^{-1}). Associated with the neutral atomic oxygen ([O]) enhancements in the high-temperature summer hemisphere (see Figures 5a and 5b), the daytime oxygen ions and electrons ([O^+] and

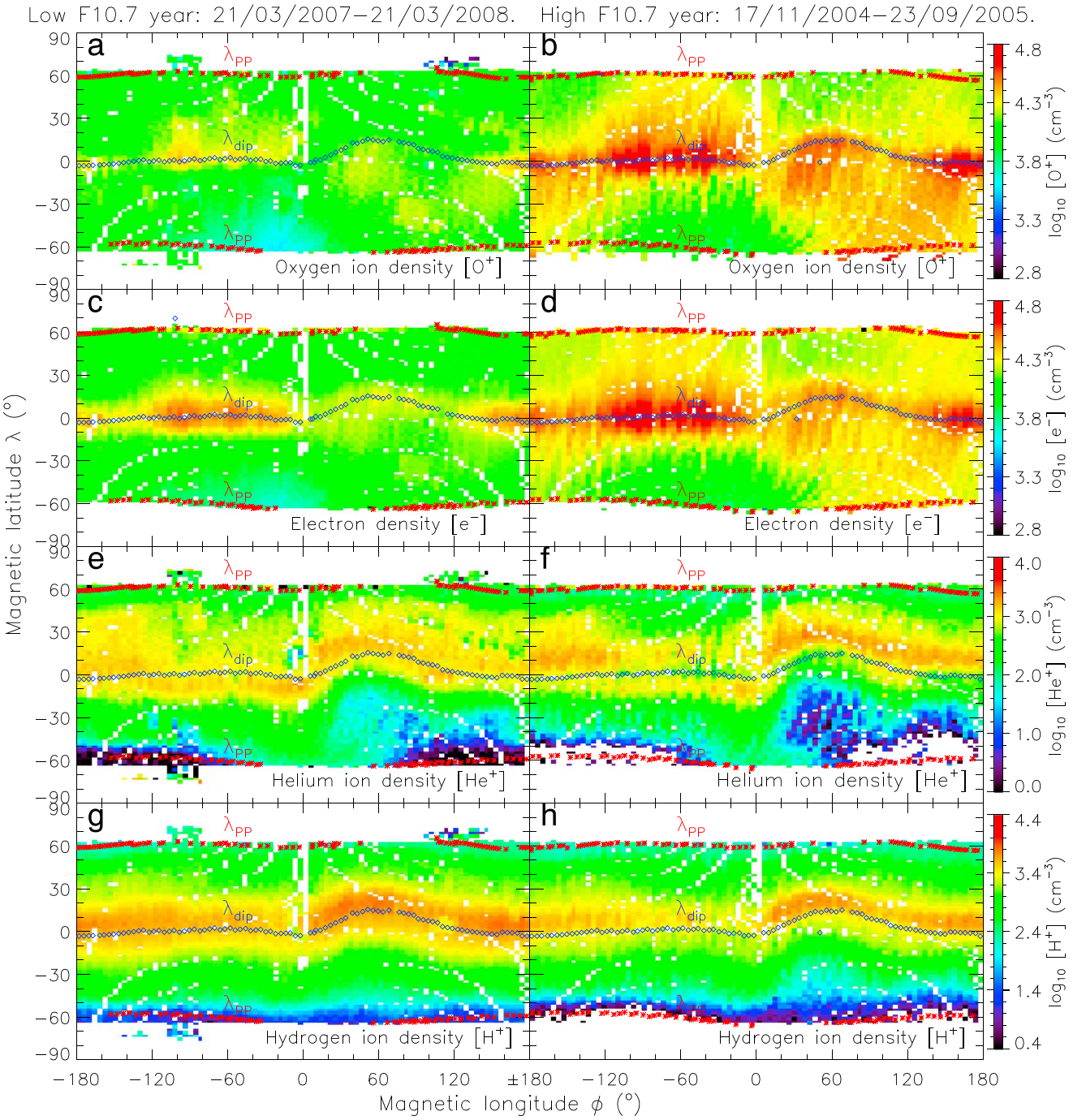

Figure 6. Solar activity ($F_{10.7}$) variations of daytime (~10:30 LT) plasma densities observed by DEMETER. The average of $F_{10.7}$ is ~ 72×10^{-22} W m^{-2} Hz^{-1} within the interval 21 March 2007 to 21 March 2008, but it increases to ~ 97×10^{-22} W m^{-2} Hz^{-1} within the interval 17 November 2004 to 23 September 2005.

[e^-]) also increase on the summerside of the dip equator (Figures 4a–4d), and their latitude distributions display the significant hemispheric asymmetry (summer dense and winter tenuous) at most longitudes, except for the low plasma densities in the WSA region ($-70° \le \lambda \le -20°$ and $-120° \le \phi \le 0°$). Although the light He^+ and H^+ ions have a maximum density (i.e., the highest [He^+] and [H^+]) at the low and middle latitudes, their densities in the winter Northern Hemisphere are much higher than the summer Southern Hemisphere. The winter enhancements of the light ions are associated with the neutral He and H enhancements in the winter hemisphere, whereas their summer depletions are associated with the increased loss

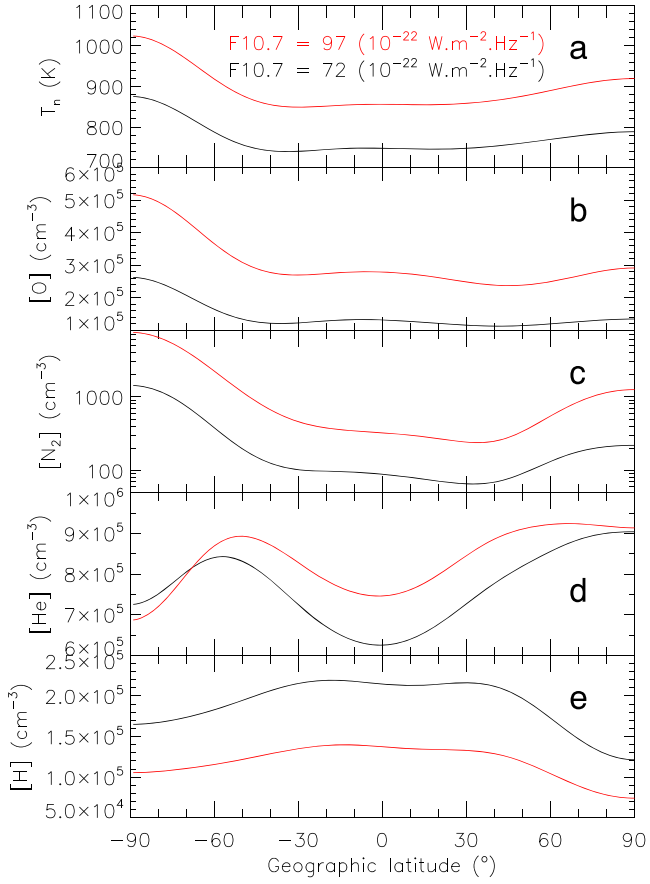

Figure 7. Annual means of the neutral composition densities at all longitudes during the low and high solar radiations (The average of $F_{10.7}$ is about 72×10^{-22} W m^{-2} Hz^{-1} in the interval 21 March 2007 to 21 March 2008, and it increases to about 97×10^{-22} W m^{-2} Hz^{-1} in the interval 17 November 2004 to 23 September 2005).

sources (e.g., [N_2], [O], and [e^-]). The charge exchange (e.g., $H + O^+ \leftrightarrow H^+ + O$) and/or recombination reactions (e.g., $He^+ + e^- \rightarrow He + h\nu$) are probably responsible for the H^+ and He^+ depletions in the summer Southern Hemisphere during the declining phase of solar activity. Moreover, other dynamic processes are also required for the dip equator-dependent semiannual variations of all plasma species.

It is necessary to point out that the semiannual means of the daytime plasma densities mainly reflect their semiannual variation tendencies. Since the neutral O density in the summer hemisphere is higher than the winter hemisphere around 22 June and 22 December, the hemispheric asymmetry of the daytime oxygen ion density should be the most prominent around two solstices. However, the latitude distributions of the neutral compositions are relatively even in both hemispheres during the vernal and autumnal equinoxes (around 21 March and 23 September). Under this circumstance, the latitude distribution of the daytime plasma density can become relatively symmetrical with respect to the dip equator around 21 March and 23 September [*Chen et al.*, 2009].

3.2. Solar Activity Variations of the Daytime Plasma and Neutral Compositions

The neutral density effect on the plasma concentration is further confirmed by the yearly averaged plasma density variations during different solar activities. Figure 6 shows the yearly averaged plasma densities ([O^+], [e^-], [He^+], and [H^+]) during the low and high solar radiations ($< F_{10.7} > \sim 72 \times 10^{-22}$ W m^{-2} Hz^{-1} in the interval 21 March 2007 to 21 March 2008 and $< F_{10.7} > \sim 97 \times 10^{-22}$ W m^{-2} Hz^{-1} in the interval 17 November 2004 to 23 September 2005). Since the semiannual effect of the neutral composition densities is removed in the yearly averaged plasma densities, the hemispheric asymmetry of all plasma species is weakened in the transition region, except for the WSA region ($-70° \le \lambda \le -20°$ and $-120° \le \phi \le 0°$) and the SAMA region ($-70° \le \lambda \le -10°$ and $0° \le \phi \le 120°$). The plasma density anomalies in the WSA and SAMA regions are due to the special plasma transports and electrodynamic effects [*He et al.*, 2009; *Horvath and Lovell*, 2009a, 2009b].

The yearly averaged plasma densities are the maximum around the dip equator ($-30° \le \lambda \le 30°$). From the solar minimum (Figures 6a, 6c, 6e, and 6g) to its declining phase (Figures 6b, 6d, 6f, and 6h), the global oxygen ions ([O^+]) and electrons ([e^-]) increase with the increasing $F_{10.7}$, whereas the hydrogen ions ([H^+]) decrease slightly with the increasing $F_{10.7}$. Unlike the O^+ and H^+ densities, the helium ion density ([He^+]) is relatively stable during different solar activities. The solar activity variations of three ion species observed by DEMETER are analogous to those observed by the SROSS C2 and FORMOSAT-1 satellites at ~500–600 km [*Borgohain and Bhuyan*, 2010].

In order to reveal the cause of the daytime plasma solar activity variations, we calculated the annual means of the neutral composition densities at all longitudes. Figure 7 displays the yearly averaged neutral composition

densities under different solar EUV radiations. The neutral temperature (T_n) increases with the enhanced solar EUV radiations ($F_{10.7}$). From the low-$F_{10.7}$ year (21 March 2007 to 21 March 2008) to the high-$F_{10.7}$ year (17 November 2004 to 23 September 2005), the neutral oxygen and nitrogen densities ([O] and [N_2]) increase ~2–4 times. The stronger solar EUV radiations ($F_{10.7}$) probably catalyze the neutral O photoionization ($O + h\upsilon \rightarrow O^+ + e^-$) and therefore lead to the [O^+] and [e^-] enhancements during the high-$F_{10.7}$ year. On the contrary, the decrease of the neutral atomic hydrogen ([H]) causes the hydrogen ion ([H^+]) reduction during the high-$F_{10.7}$ year. Although the increased neutral helium ([He]) can produce more helium ions during the high-$F_{10.7}$ year, the newborn helium ions are also lost because of the charge exchange ($N_2 + He^+ \leftrightarrow N_2^+ + He$) with the increasing neutral nitrogen ([N_2]) or the recombination ($He^+ + e^- \rightarrow He + h\nu$) with the increasing electrons. The photochemical balance between the He^+ production and loss can maintain a relatively stable He^+ concentration during different solar activities. These results demonstrate that the neutral composition densities also influence their ion concentrations during different solar activities. Even in the same year, the oxygen ion density ([O^+]) is also higher than that of the hydrogen ions ([H^+]) in the same region, as the oxygen ions have more neutral sources than the hydrogen ions (i.e., [O] > [H]). The higher oxygen ion content ([O^+]) at the DEMETER orbit (~670–710 km) agrees with the previous observations and models at 600–850 km [*Truhlík et al.*, 2005; *Horvath and Lovell*, 2009a].

4. Discussions

The neutral composition densities mainly influence the local plasma production and loss rates via the photoionization or charge exchange reactions. Moreover, the plasma production rate also depends on the solar zenith angle, photon flux, absorption cross section, and ionization efficiency [*Schunk and Nagy*, 2009]. The influence of solar zenith angle or photon flux is the same for all plasma species at the same location. If different neutral compositions (O, He, and H) have the same absorption cross section and ionization efficiency, the latitude distribution of the plasma production rate or density depends on the neutral composition density. Thus, the semiannually latitudinal variation of the daytime oxygen ion density ([O^+]) is mainly determined by that of neutral atomic oxygen density ([O]).

However, the latitude distributions of the He^+ and H^+ ions do not fully depend on the neutral He and H, indicating that the latitude distributions of the light He^+ and H^+ ions are also modified by the neutral wind drags or other electromagnetic forces relative to the configuration of geomagnetic field. The neutral wind drags are due to the neutral composition collisions with different plasma species. Collisional interactions between plasma and neutrals can be resonant or nonresonant [*Schunk and Nagy*, 1980, 2009]. For a given ion-neutral pair, the collision frequencies of the resonant and nonresonant ion-neutral interactions are expressed as [*Schunk and Nagy*, 1980, 2009]

$$v_{\text{in}} = \frac{8}{3\sqrt{\pi}} N_n \left[\frac{2k(T_i + T_n)}{m_i}\right]^{\frac{1}{2}} [A + 3.96A_1 - A_1 \log_{10}(T_i + T_n)]^2 \text{ for resonant case and} \quad (1)$$

$$v_{\text{in}} = C_{\text{in}} N_n \text{ for nonresonant case} \quad (2)$$

where A and A_1 are constants, N_n is the number density of neutral compositions, and C_{in} is a numerical coefficient. The reduced expressions of the v_{in} and C_{in} have been given by Tables 4.4–4.6 in the textbook of ionosphere [*Schunk and Nagy*, 2009].

Besides the plasma-neutral collisions, Coulomb collisions between the charged particles can also change the plasma velocity distributions in the parallel and perpendicular directions [*Nanbu*, 1997] and therefore influence the particle trapping and latitude distribution [*Wilson et al.*, 1992; *Wang et al.*, 2015]. The Coulomb collision frequency (v_{st}) for the interactions between different ion species (s and t) can be expressed as [*Schunk and Nagy*, 2009]

$$v_{st} = B_{st} \frac{n_t}{T_t^{3/2}} \quad (3)$$

Here B_{st} is a numerical coefficient that is given in Table 4.3 in the textbook of ionospheres [*Schunk and Nagy*, 2009]. n_t is the ion number density (n_t = [O^+], [He^+], or [H^+] in cm^{-3}) and T_t the temperature ($T_t = T_i$ in kelvin).

Table 1. Gyrofrequency of Charged Particles, the Average Plasma-Neutral Collision Frequencies, and the Coulomb Collision Frequencies of Different Plasma Species at ~670 km

Plasma Species	Gyrofrequency (f_c in Hz)	Collision Frequencies for the Plasma-Neutral Interactions ($<\nu_{in}>$ in s^{-1})			Coulomb Collision Frequency of Different Plasma Species (ν_{ei} and ν_{st} in s^{-1})		
		H	He	O	H^+	He^+	O^+
e^-	5.3×10^5	2.7×10^{-2}	2.1×10^{-2}	2.3×10^{-3}	4.8×10^{-1}	1.4×10^{-1}	2.98
H^+	28.8	9.9×10^{-4}	8.1×10^{-4}	2.8×10^{-4}	2.2×10^{-2}	8.26×10^{-3}	1.89×10^{-1}
He^+	7.2	8.9×10^{-5}	1.2×10^{-3}	1.4×10^{-4}	6.9×10^{-3}	3.26×10^{-3}	8.77×10^{-2}
O^+	1.8	2.6×10^{-5}	1.0×10^{-4}	1.2×10^{-4}	1.9×10^{-3}	1.01×10^{-3}	3.39×10^{-2}

Similarly, the Coulomb collision frequencies for the electron-ion interactions (ν_{ei}) and the electron-electron interactions (ν_{ee}) can also be approximately expressed as [*Schunk and Nagy*, 2009]

$$\nu_{ei} = 54.5\frac{n_i Z_i^2}{T_e^{3/2}} \text{ and} \tag{4}$$

$$\nu_{ee} = \frac{54.5}{\sqrt{2}}\frac{n_e}{T_e^{3/2}} \tag{5}$$

Here Z_i is the ion charge number, $n_i = [O^+]$, $[He^+]$, or $[H^+]$ (in cm^{-3}), n_e is the electron number density ($n_e = [e^-]$ in cm^{-3}), and T_e is the electron temperature (in kelvin).

Using the plasma data from DEMETER and the neutral data from the NRLMSISE-00 model, we calculated the average collision frequencies for the plasma-neutral interactions at ~670 km (where the average ion temperature $< T_i > \sim 1794.2$ K) and estimated the Coulomb collision frequencies of different plasma species. Table 1 shows the gyrofrequency ($f_c = q_i/2\pi m_i$) of each plasma species, the average plasma-neutral collision frequencies ($<\nu_{in}>$ in s^{-1}), and the Coulomb collision frequencies (ν_{ei} and ν_{st} in s^{-1}) of different plasma species at ~670 km. In the transition region, the gyrofrequencies of the ions and electrons are greater than the plasma-neutral collision frequencies and the Coulomb collision frequencies. The lower plasma-neutral collision frequencies suggest that the neutral wind drags are negligible in the transition region above 670 km. However, the Coulomb collision frequencies between the light plasma species (e^-, H^+, and He^+) with the heavy oxygen ions (O^+) are still high at 670 km. The frequent Coulomb collisions can cause the pitch angle scatterings of the charged particles [*Wang et al.*, 2015].

In the semikinetic approximation, each ion species (O^+, H^+, and He^+) can be treated as single particles in the weak plasma-neutral collision region, and the field-aligned or latitudinal motion of three ion species depends on the field-aligned electric field, gravitational force, magnetic mirror force, and centrifugal force along the magnetic field lines [*Wang et al.*, 2015]. Based on the field-aligned motion equations of the charged particles [*Wang et al.*, 2015], the field-aligned acceleration ($a_{i||} = dv_{i||}/dt$) of each ion species (i) is given by

$$a_{i||} = \frac{q_i}{m_i}\mathbf{E}_{||} - g|\sin I| - \frac{\mu_i}{m_i}\frac{\partial B}{\partial s} + \mathbf{U}_E \cdot \left(\frac{\partial \hat{b}}{\partial t} + v_{||}\frac{\partial \hat{b}}{\partial s} + \mathbf{U}_E \cdot \nabla \hat{b}\right) \tag{6}$$

Here q_i and m_i are the particle electric charge and mass, respectively. $\mathbf{E}_{||}$ is the electric field component parallel or antiparallel to the magnetic field vector $\mathbf{B}$. $g|\sin I|$ is the gravitational acceleration along the magnetic field lines, and I is the magnetic inclination. B is the magnitude of magnetic field, and $\hat{b} = \frac{\mathbf{B}}{B}$ (the unit vector of the magnetic field). s is the particle position along the magnetic field line, and μ_i is the magnetic moment. $\mathbf{U}_E$ is the drift velocity of the flux tube at position s perpendicular to the magnetic field, and $\mathbf{U}_E = \mathbf{E}\times\mathbf{B}/B^2$ ($\mathbf{E}$ is the eastward or convection electric field). $v_{||}$ is the particle velocity parallel or antiparallel to $\mathbf{B}$.

Since the electric field force ($q_i\mathbf{E}_{||}$) depends on the particle electric charge polarity, the same electric field makes ions and electrons move in the opposite directions. The equatorial accumulations of the light ions and electrons indicate that the electric field force is negligible at 670–710 km. Therefore, the equatorial accumulations of the light ions and electrons are mainly due to the equatorward forces independent of the particle electric charge polarity (e.g., the magnetic mirror force and centrifugal force along the magnetic field lines). For a dipolar magnetic field configuration, the charged particles bouncing along a magnetic field

line have a vertex height near the dip equator, and their gravitational acceleration ($g|\sin I|$) along the field line is negligible at the vertex height (where $\sin I \sim 0$). However, at the middle and high latitudes of both hemispheres, the charged particles have to simultaneously undergo the poleward/downward gravitational force ($g|\sin I|$), equatorward magnetic mirror force ($-\mu_i \frac{\partial B}{\partial s}$), and centrifugal force along the magnetic field lines.

Each force effect on the three ion species (O^+, H^+, and He^+) has been simulated through a dynamic fluid-kinetic model [*Wang et al*., 2015]. Their simulation results show that the latitudinal motions of the light H^+ and He^+ ions are mainly dominated by the equatorward magnetic mirror force and centrifugal force along the field lines, whereas the gravity does not play an important role in the field-aligned motion of the light ions. As a consequence, most of the light ions (H^+ and He^+) can be transported to the dip equator and are trapped at low magnetic latitudes through the Coulomb collisions. This point is fully proved by the equatorial accumulations of the light plasma species (He^+, H^+, and e^-) observed by DEMETER. However, our observations indicate that the high-density He^+ or H^+ ions sometimes only appear on the winterside of the dip equator (see Figures 1 and 4). The hemispheric asymmetry of the high-density He^+ or H^+ ions is associated with the hemispheric asymmetric distributions of their neutral sources ([He] or [H]) and loss sources ([N_2] and [O]) (see Figures 3 and 5). Therefore, the photoionization or charge exchange reactions of the neutral atmospheric compositions can also influence the latitude distributions of the light plasma species in different seasons.

The role of photochemical reactions becomes more significant for the heavy oxygen ions. Since the heavy oxygen ions (O^+) do not have enough kinetic energy to reach the equator [*Wang et al*., 2015], most of the newborn oxygen ions can be trapped in the summer hemispheric source region through the Coulomb collisions. The summer enhancement of the heavy oxygen ions is consistent with the neutral O enhancement in the summer hemisphere, suggesting that the large gravitational force ($m_i g|\sin I|$) of the oxygen ions probably counteract the equatorward magnetic mirror force and centrifugal force along the magnetic field lines.

5. Summary and Conclusions

For the first time, the multiple-species plasma measurements by DEMETER demonstrate that the semiannually latitudinal variation of the heavy oxygen ions (O^+) is different from those of the light plasma species (He^+, H^+, and e^-) in the dayside transition region above 670 km, where the plasma-neutral collision frequencies are very low ($<0.03\,s^{-1}$) but the Coulomb collision frequencies of the light plasma species are high (~0.09–2.98 s^{-1}). Owing to the photoionization ($O + h\upsilon \rightarrow O^+ + e^-$) of neutral atomic oxygen (O) increasing in summer, the daytime oxygen ions basically increase on the summerside of the dip equator, and the oxygen ion density has significantly the summer-dense and winter-tenuous hemispheric asymmetry with respect to the dip equator. Although the neutral oxygen photoionization can also produce more electrons (e^-) in the summer hemisphere, the high-density electrons mainly accumulate around the dip equator at most longitudes.

Unlike the semiannual variation of the heavy oxygen ions, the daytime helium ions (He^+) with a lighter mass often increase on the winterside of the dip equator, and the helium ion density ([He^+]) has the winter-dense and summer-tenuous hemispheric asymmetry with respect to the dip equator. The high-density helium ions on the winterside are associated with the neutral atomic helium (He) enhancement in the winter hemisphere. Although the neutral atomic hydrogen (H) also seasonally increases in the winter hemisphere, the daytime hydrogen ions (H^+) with the lightest mass can maintain a maximum density around the dip equator ($|\lambda| < 30°$). When there are more neutral atomic oxygen in the summer Southern Hemisphere, the hydrogen ion density ([H^+]) on the winterside sometimes is also higher than that on the summerside. These results indicate that the photoionization (e.g., $He + h\upsilon \rightarrow He^+ + e^-$) and charge exchange reaction (e.g., $H + O^+ \leftrightarrow H^+ + O$) of the seasonally changed neutral He and H are still the important causes of the light ion production and loss in the transition region. However, the latitude distributions of the high-density He^+ and H^+ ions do not fully depend on the high-density neutral He and H. The equatorial maximum densities of the light plasma species (He^+, H^+, and e^-) indicate that the light charged particles are easily transported by some equatorward forces (e.g., the magnetic mirror force and centrifugal force). The frequent Coulomb collisions between the charged particles probably lead to the trappings of the light plasma species around the dip equator.

Moreover, the neutral composition densities also influence their ion concentrations during different solar activities. From the low-$F_{10.7}$ year (2007–2008) to the high-$F_{10.7}$ year (2004–2005), the daytime oxygen ions and electrons increase with the increasing neutral atomic oxygen, whereas the daytime hydrogen ions tend to decrease with the decreasing neutral atomic hydrogen. In contrast to the clear $F_{10.7}$-dependent variations of the oxygen and hydrogen ions, the daytime helium ion density has no obvious solar activity variation, suggesting that the generation (via the neutral He photoionization) and loss (via the charge exchange with neutral nitrogen N_2 and/or the recombination with electrons) of the daytime He^+ ions are comparable during different solar activities.

Acknowledgments
This work is supported by the NSFC (41374165, 41431071, and 41074119). DEMETER IAP/ISL data are available at the Web site http://demeter.cnrs-orleans.fr. The geomagnetic and solar indices (*Kp*, *Dst*, *AE*, and $F_{10.7}$) are available at the Web site http://cdaweb.gsfc.nasa.gov/sp_phys. The NRLMSISE-00 model is available at the Web site http://ccmc.gsfc.nasa.gov/modelweb. Authors thank all staffs working for the data used in this paper.

References

Anderson, D. N. (1973), A theoretical study of the ionospheric *F*-region equatorial anomaly, II. Results in the American and Asian sectors, *Planet. Space Sci.*, *21*, 421–442, doi:10.1016/0032-0633(73)90041-X.

Aponte, N., C. G. M. Brum, M. P. Sulzer, and S. A. González (2013), Measurements of the O^+ to H^+ transition height and ion temperatures in the lower topside ionosphere over Arecibo for equinox conditions during the 2008–2009 extreme solar minimum, *J. Geophys. Res. Space Physics*, *118*, 4465–4470, doi:10.1002/jgra.50416.

Balan, N., P. K. Rajesh, S. Sripathi, S. Tulasiram, J. Y. Liu, and G. J. Bailey (2013), Modeling and observations of the north–south ionospheric asymmetry at low latitudes at long deep solar minimum, *Adv. Space Res.*, *52*, 375–382.

Berthelier, J. J., M. Godefroy, F. Leblanc, E. Seran, D. Peschard, P. Gilbert, and J. Artru (2006), IAP, the thermal plasma analyzer on DEMETER, *Planet. Space Sci.*, *54*, 487–501.

Borgohain, A., and P. K. Bhuyan (2010), Solar cycle variation of ion densities measured by SROSS C2 and FORMOSAT-1 over Indian low and equatorial latitudes, *J. Geophys. Res.*, *115*, A04309, doi:10.1029/2009JA014424.

Chao, C. K., and S.-Y. Su (2000), Charged particle motion inside the retarding potential analyzer, *Phys. Plasmas*, *7*, 101–107, doi:10.1063/1.873817.

Chen, Y., L. Liu, W. Wan, X. Yue, and S.-Y. Su (2009), Solar activity dependence of the topside ionosphere at low latitudes, *J. Geophys. Res.*, *114*, A08306, doi:10.1029/2008JA013957.

Denton, M. H., G. J. Bailey, C. R. Wilford, A. S. Rodger, and S. Venkatraman (2002), He^+ dominance in the plasmasphere during geomagnetically disturbed periods: 1. Observational results, *Ann. Geophys.*, *20*, 461–470.

Gladyshev, V. A., A. Y. Shchekotov, N. V. Yagova, J.-J. Berthelier, M. Parrot, O. S. Akent'eva, L. N. Baranskii, E. N. Fedorov, T. M. Mulyarchik, and O. A. Molchanov (2012), Concentration of ions in the topside ionosphere as measured onboard the DEMETER satellite: Morphology and dependence on solar and geomagnetic activity, *Cosmic Res.*, *50*(2), 103–115.

He, M., L. Liu, W. Wan, B. Ning, B. Zhao, J. Wen, X. Yue, and H. Le (2009), A study of the Weddell Sea Anomaly observed by FORMOSAT-3/COSMIC, *J. Geophys. Res.*, *114*, A12309, doi:10.1029/2009JA014175.

Heelis, R. A., W. R. Coley, A. G. Burrell, M. R. Hairston, G. D. Earle, M. D. Perdue, R. A. Power, L. L. Harmon, B. J. Holt, and C. R. Lippincott (2009), Behavior of the O^+/H^+ transition height during the extreme solar minimum of 2008, *Geophys. Res. Lett.*, *36*, L00C03, doi:10.1029/2009GL038652.

Horvath, I., and B. C. Lovell (2009a), Distinctive plasma density features of the topside ionosphere and their electrodynamics investigated during southern winter, *J. Geophys. Res.*, *114*, A01304, doi:10.1029/2008JA013683.

Horvath, I., and B. C. Lovell (2009b), Investigating the relationships among the South Atlantic Magnetic Anomaly, southern nighttime midlatitude trough, and nighttime Weddell Sea Anomaly during southern summer, *J. Geophys. Res.*, *114*, A02306, doi:10.1029/2008JA013719.

Lebreton, J.-P., et al. (2006), The ISL Langmuir probe experiment processing onboard DEMETER: Scientific objectives, description and first results, *Planet. Space Sci.*, *54*, 472–486.

Lei, J., T. Matsuo, X. Dou, E. Sutton, and X. Luan (2012), Annual and semiannual variations of thermospheric density: EOF analysis of CHAMP and GRACE data, *J. Geophys. Res.*, *117*, A01310, doi:10.1029/2011JA017324.

Li, L. Y., J. B. Cao, G. C. Zhou, T. L. Zhang, D. Zhang, I. Dandouras, H. Rème, and C. M. Carr (2011a), Multiple responses of magnetotail to the enhancement and fluctuation of solar wind dynamic pressure and the southward turning of interplanetary magnetic field, *J. Geophys. Res.*, *116*, A12223, doi:10.1029/2011JA016816.

Li, L. Y., J. Y. Yang, J. B. Cao, L. Lu, Y. Wu, and D. M. Yang (2011b), Statistical backgrounds of topside-ionospheric electron density and temperature and their variations during geomagnetic activity [in Chinese], *Chinese J. Geophys.*, *54*(10), 2437–2444, doi:10.3969/j.issn.0001-5733.

Liu, H., C. Stolle, M. Förster, and S. Watanabe (2007a), Solar activity dependence of the electron density at 400 km at equatorial and low latitudes observed by CHAMP, *J. Geophys. Res.*, *112*, A11311, doi:10.1029/2007JA012616.

Liu, L., W. Wan, B. Ning, O. M. Pirog, and V. I. Kurkin (2006), Solar activity variations of the ionospheric peak electron density, *J. Geophys. Res.*, *111*, A08304, doi:10.1029/2006JA011598.

Liu, L., B. Zhao, W. Wan, S. Venkartraman, M.-L. Zhang, and X. Yue (2007b), Yearly variations of global plasma densities in the topside ionosphere at middle and low latitudes, *J. Geophys. Res.*, *112*, A07303, doi:10.1029/2007JA012283.

Liu, L., B. Zhao, W. Wan, B. Ning, M.-L. Zhang, and M. He (2009), Seasonal variations of the ionospheric electron densities retrieved from Constellation Observing System for Meteorology, Ionosphere, and Climate mission radio occultation measurements, *J. Geophys. Res.*, *114*, A02302, doi:10.1029/2008JA013819.

Luan, X., and S. C. Solomon (2008), Meridional winds derived from COSMIC radio occultation measurements, *J. Geophys. Res.*, *113*, A08302, doi:10.1029/2008JA013089.

MacPherson, B., S. A. González, G. J. Bailey, R. J. Moffett, and M. P. Sulzer (1998), The effects of meridional neutral winds on the O^+-H^+ transition altitude over Arecibo, *J. Geophys. Res.*, *103*(A12), 29,183–29,198, doi:10.1029/98JA02660.

Mauersberger, K. W., W. E. Potter, and D. C. Kayser (1976), A direct measurement of the winter helium bulge, *Geophys. Res. Lett.*, *3*, 269–271, doi:10.1029/GL003i005p00269.

Moldwin, M. B., L. Downward, H. K. Rassoul, R. Amin, and R. R. Anderson (2002), A new model of the location of the plasmapause: CRRES results, *J. Geophys. Res.*, *107*(A11), 1339, doi:10.1029/2001JA009211.

Murphy, J. A., A. E. Sutton, and R. A. Heelis (1984), The influence of neutral winds on He^+ distributions in the equatorial ionospshere, *Planet. Space Sci.*, *32*(5), 543–550.

Nanan, B., C. Y. Chen, P. K. Rajesh, J. Y. Liu, and G. J. Bailey (2012), Modeling and observations of the low latitude ionosphere-plasmasphere system at long deep solar minimum, *J. Geophys. Res.*, *117*, A08316, doi:10.1029/2012JA017846.

Nanbu, K. (1997), Theory of cumulative small-angle collisions in plasmas, *Phys. Rev. E*, *55*, 4642–4652, doi:10.1103/PhysRevE.55.4642.
Picone, J. M., A. E. Hedin, D. P. Drob, and A. C. Aikin (2002), NRLMSISE-00 empirical model of the atmosphere: Statistical comparisons and scientific issues, *J. Geophys. Res.*, *107*(A12), 1468, doi:10.1029/2002JA009430.
Rich, F. J., P. J. Sultan, and W. J. Burke (2003), The 27-day variations of the plasma densities and temperatures in the topside ionosphere, *J. Geophys. Res.*, *108*(A7), 1297, doi:10.1029/2002JA009731.
Schunk, R. W., and A. F. Nagy (1980), Ionospheres of the terrestrial planets, *Rev. Geophys. Space Phys.*, *18*, 813–852, doi:10.1029/RG018i004p00813.
Schunk, R. W., and A. F. Nagy (2009), *Ionospheres: Physics, Plasma Physics, and Chemistry*, 2nd ed., Cambridge Univ. Press, Cambridge.
Song, P., and V. M. Vasyliūnas (2013), Inductive-dynamic coupling of the ionosphere with the thermosphere and the magnetosphere, in *Modeling the Ionosphere-Thermosphere System*, *Geophys. Monogr. Ser.*, vol. 201, edited by J. Huba and R. W. Schunk, 360 pp., AGU, Washington, D. C.
Song, P., T. I. Gombosi, and A. D. Ridley (2001), Three-fluid Ohm's law, *J. Geophys. Res.*, *106*, 8149–8156, doi:10.1029/2000JA000423.
Song, P., V. M. Vasyliūnas, and X.-Z. Zhou (2009), Magnetosphere-ionosphere/thermosphere coupling: Self-consistent solutions for a one-dimensional stratified ionosphere in three-fluid theory, *J. Geophys. Res.*, *114*, A08213, doi:10.1029/2008JA013629.
Su, S.-Y., C. K. Chao, H. C. Yeh, and R. A. Heelis (2005), Seasonal and latitude distributions of the dominant light ions at 600 km topside ionosphere from 1999 to 2002, *J. Geophys. Res.*, *110*, A01302, doi:10.1029/2004JA010564.
Taylor, H. A., H. G. Mayr Jr., and H. C. Brinton (1970), Observations of hydrogen and helium ions during a period of rising solar activity, *Space Res.*, *10*, 663–673.
Torr, D. G., and M. R. Torr (1978), Chemistry of the thermosphere and ionosphere, *J. Atmos. Terr. Phys.*, *41*, 797–839.
Truhlík, V., L. Třískova, and J. Šmilauer (2005), Manifestation of solar activity in the global topside ion composition—A study based on satellite data, *Ann. Geophys.*, *23*, 2511–2517.
Tu, J., P. Song, and V. M. Vasyliūnas (2014), Inductive-dynamic magnetosphere-ionosphere coupling via MHD waves, *J. Geophys. Res. Space Physics*, *119*, 530–547, doi:10.1002/2013JA018982.
Wang, X., J. J. Berthelier, and J. P. Lebreton (2010), Ionosphere variations at 700 km altitude observed by the DEMETER satellite during the 29 March 2006 solar eclipse, *J. Geophys. Res.*, *115*, A11312, doi:10.1029/2010JA015497.
Wang, Y., J. Tu, and P. Song (2015), A new dynamic fluid-kinetic model for plasma transport within the plasmasphere, *J. Geophys. Res. Space Physics*, *120*, 8486–8502, doi:10.1002/2015JA021345.
Wilson, G. R., J. L. Horwitz, and J. Lin (1992), A semikinetic model for early stage plasmasphere refilling: 1, Effects of Coulomb collisions, *J. Geophys. Res.*, *97*(A2), 1109–1119, doi:10.1029/91JA01459.
Weiss, A. (1953), The structure of the *F* region of the ionosphere, *Aust. J. Phys.*, *6*, 291–303.
Yu, Y., and A. Ridley (2013a), Exploring the effect of ionospheric heavy ion outflow on magnetospheric dynamics: The effect of outflow intensity, *J. Geophys. Res. Space Physics*, *118*, 5522–5531, doi:10.1029/jgra.50528.
Yu, Y., and A. Ridley (2013b), Exploring the effect of ionospheric heavy ion outflow on magnetospheric dynamics: Dependence of source location, *J. Geophys. Res. Space Physics*, *118*, 1711–1722, doi:10.1029/2012JA018411.
Yue, X., W. S. Schreiner, J. Lei, C. Rocken, Y. Kuo, and W. Wan (2010), Climatology of ionospheric upper transition height derived from COSMIC satellites during the solar minimum of 2008, *J. Atmos. Terr. Phys.*, *72*, 1270–1274, doi:10.1016/j.jastp.2010.08.018.